COBEM 2021 26th International Congress of Mechanical Engineering
November 22-26, 2021, Virtual Congress, Brazil
ABCM Associação Brasileira de Engenharia e Ciências Mecânicas

COB-2021-0295
NONLINEAR ENERGY SINK AS A PASSIVE CONTROL APPROACH TO SUPPRESS AIRFOIL FLUTTER

Adolfo Esteves Ribeiro
adolforibeiro@usp.br
José Augusto Ignácio da Silva
j.i.silva@usp.br
Flávio D. Marques
fmarques@sc.usp.br

Department of Mechanical Engineering
São Carlos School of Engineering
University of São Paulo
Avenida Trabalhador São-carlense, 400, 13566-590, São Carlos, SP, Brazil

Abstract. *Aeroelastic systems can be subjected to a self-excited mechanism and experience the so-called phenomenon of flutter. Under this condition, airfoils can exhibit self-sustained oscillations with exponential trends diverging to infinity, characterizing an unstable system's behavior. The high vibration levels can lead to fatigue and catastrophic failure, thereby justifying flutter suppression schemes. This work proposes an investigation about vibration absorbers known as Nonlinear Energy Sinks (NES) to suppress aeroelastic instabilities in a pitch and plunge typical section. Unsteady aerodynamic loads are modeled according to generalized Theodorsen's and Wagner's theories, represented in state space. The aeroelastic model is assumed linear. A conventional NES approach is considered, in which a pure cubic stiffness spring is adopted. A parametric study involving the physical parameters of the NES and its positioning in the airfoil is conducted to find conditions that efficiently favor the target energy transfer (TET) concept for the NES. This study assesses each parameter's sensitivity aiming for a future investigation by employing an optimization process in the NES design.*

Keywords: *Flutter, Flutter passive control, Nonlinear energy sinks, Typical aeroelastic section, Target energy transfer.*

1. INTRODUCTION

Aeroelastic systems can operate in self-excited regimes, characterizing the so-called phenomenon of flutter. Under the aforementioned conditions, one can observe self-sustained oscillations represented by the coupling of two or more structural vibration modes; in the model later exposed, the pitch and plunge modes are responsible for oscillating (Fung, 1995). When dealing with linear models, the self-excited oscillations diverge exponentially, causing the system to be unstable. However, inserting non-linear features in the system could modify its behaviour, resulting in an equilibrium state or even limit cycle oscillations (LCOs)(Nayfeh and Balachandran, 1995).

Flutter, linear or non-linear, induces unwanted high levels of vibration on the aircraft, followed by fatigue and catastrophic failure of structural components. Knowing that, diverse techniques of both active and passive control have been adopted during the years to try and suppress those instabilities; particularly, the use of nonlinear energy sinks (NES) are of great interest for its capability of absorbing large amplitude and resonant oscillations. The NES comprises of a dynamic vibration absorber with non-linear characteristics and a few different construction methods, between those: cubic spring (Lee *et al.*, 2007), hysteresis (Tsiatas and Charalampakis, 2018), bistable spring (Al-Shudeifat, 2014), rotary inertial mass (Saeed *et al.*, 2019), among others. This device type has the intrinsic function of performing a target energy transfer (TET) from the primary structure, apart from being more robust when compared to the classic dynamic vibration absorber.

Lee *et al.* (2007) analysed the cubic spring NES dealing with an aeroelastic problem, using the complex average method and an energy flux investigation. Luongo and Zulli (2014) used the method of multiple scales coupled with the harmonic balance method to observe a similar system. Guo *et al.* (2018) used this last method on the clearance located on a 2D airfoil control surface. Pacheco *et al.* (2018) used NES for mitigating the vibration on supersonic panels.

The model chosen for this study was the cubic spring NES linked with a 2 degrees of freedom (DOFs) typical section when modelling the airfoil, while the aerodynamic loads were taken into account through Theodorsen's approximation (Theodorsen, 1935). On a first glance, nonlinearities are not taken into account so the dynamical system behaviour can be seen more clearly. Followed by that, a parametric study encompassing values from both the typical section and the NES has been made in order to compute each parameter's sensibility, also being a first step for a future optimization process.

2. AEROELASTIC MODEL

The aeroelastic model comprises of a typical section with two degrees-of-freedom and a NES ideally fixed inside of the profile section. The airfoil can move in pitch, $\alpha(t)$, and plunge, $h(t)$ (positive downwards), while the NES device has a displacement relative to the main structure referred to by $w(t)$. Figure 1 shows the dynamic system used for modeling the problem.

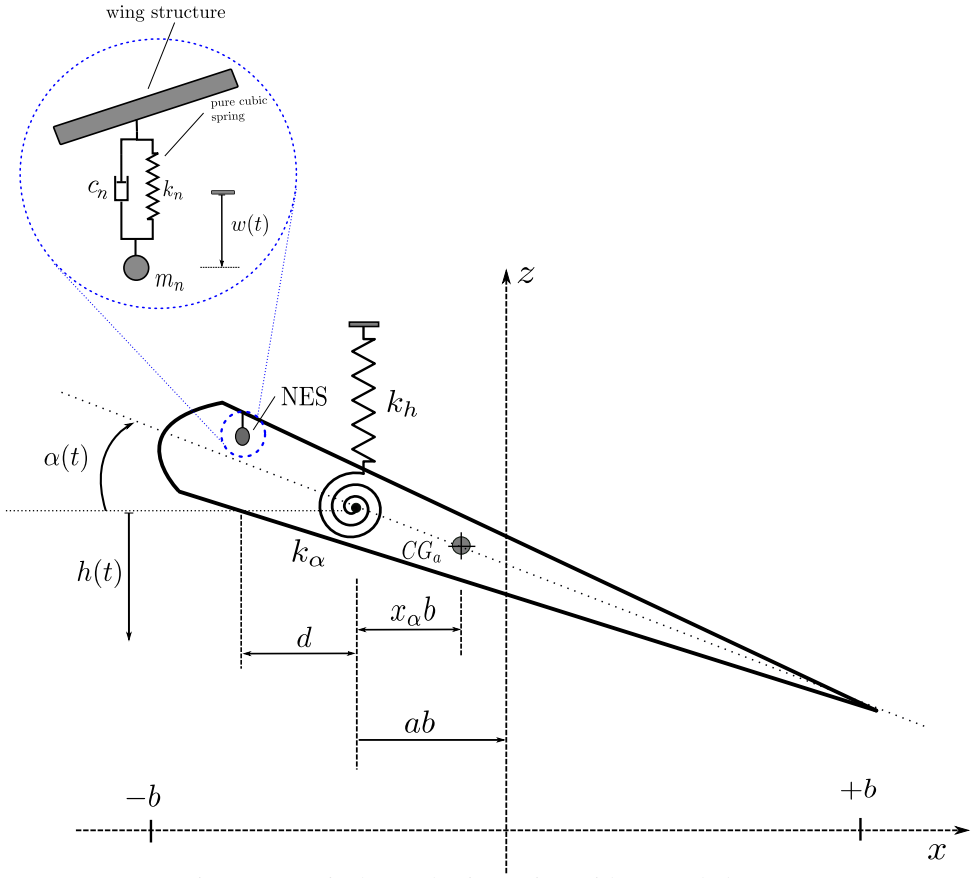

Figure 1: Typical aeroelastic section with a coupled NES.

The coordinate system was chosen in a way that x = 0 is located at the airfoil's center and the chord has a value of $2b$. The elastic axis is at a distance ab from the origin and $x_\alpha b$ from the center of gravity (CG_α), $x_\alpha = S_\alpha/mb$ is the distance between the elastic axis and the CG_α (where S_α is the static moment). At the elastic axis, there are linear springs for the pitch and plunge motions with constants k_α and k_h, respectively. The linear damping is given by constants c_α and c_h referring to pitch and plunge degrees-of-freedom, respectively. For the NES modeling, it is ideally placed inside the airfoil at a distance d from the elastic axis and its coefficients are k_n for the pure cubic stiffness and c_n for the linear damping. Other values defining the typical section are: a mass per unit of length m, mass moment of inertia I_α, static moment S_α, and the mass m_n for the NES device. Airflow of velocity U has been considered to act over the system, resulting in unsteady loads, namely, a lift force, $L(t)$, and a pitching moment, M_α, acting on the elastic axis.

In dimensionless format, the equations of motion are given by:

$$\begin{aligned}
&\mu_e\ddot{\xi}(t) + x_\alpha\ddot{\alpha}(t) + 2\zeta_h\omega_h\dot{\xi}(t) + \omega_h^2\xi - 2\theta_n\zeta_h\omega_h\dot{\upsilon}(t) - \gamma_n\omega_h^2\upsilon^3(t) = -L(t)/mb \ ; \\
&r_\alpha^2\ddot{\alpha}(t) + x_\alpha\ddot{\xi}(t) + 2r_\alpha^2\zeta_\alpha\omega_\alpha\dot{\alpha}(t) + r_\alpha^2\omega_\alpha^2\alpha + 2\delta\theta_n\zeta_h\omega_h\dot{\upsilon}(t) + \delta\gamma_n\omega_h^2\upsilon^3(t) = M_\alpha(t)/mb^2 \ ; \\
&\mu_n\left(\ddot{\upsilon}(t) + \ddot{\xi}(t) - \delta_n\ddot{\alpha}(t)\right) + 2\theta_n\zeta_h\omega_h\dot{\upsilon}(t) + \gamma_n\omega_h^2\upsilon^3(t) = 0 \ ;
\end{aligned} \tag{1}$$

where $\xi = h(t)/b$ is the dimensionless plunge displacement (positive downwards), $\upsilon(t) = w(t)/b$ is the NES relative displacement, $\theta_n = c_n/c_h$ is the ratio between the NES and plunge damping, $\lambda_n = c_n/m$ is the NES' damping, $\gamma_n = k_n b^2/m$ is the dimensionless cubic stiffness, $\delta_n = d/b$ is the NES' location in chord length, $\mu_n = m_n/m$ is the NES' dimensionless mass, $\mu_e = m_T/m$ is the system's dimensionless mass, $r_\alpha^2 = I_\alpha/mb^2$ is the radius of gyration (where I_α is the mass moment of inertia w.r.t. the CG_α), $\omega_h^2 = k_h/m$ and $\omega_\alpha = k_\alpha/I_\alpha$ are the plunge and pitch uncoupled natural frequencies, respectively, and $\zeta_h = c_h/2m\omega_h$ and $\zeta_\alpha = c_h/2m\omega_\alpha$ are the plunge and pitch damping ratio, respectively.

Generalizing Theodorsen's approach (Theodorsen, 1935) for the unsteady aerodynamic loading model made it possible to compute both $L(t)$ and $M(t)$. The reduced frequency function can be expanded using the indicial response given by Wagner's function (Fung, 1995), followed by applying the Padé interpolation approach, which results in an augmented aerodynamic states formulation (Vasconcellos *et al.*, 2012). By grouping and expanding the terms corresponding to the aerodynamic load, the final set of equations of motion governing the typical aeroelastic section coupled with a NES is:

$$\begin{aligned}
&\mathbf{M}_T\ddot{\mathbf{x}}_s + \mathbf{B}_T\dot{\mathbf{x}}_s + \mathbf{K}_T\mathbf{x}_s - \mathbf{A}_1\mathbf{x}_a - 2\theta_n\zeta_h\omega_h\hat{\mathbf{N}}\dot{v}(t) - \gamma_n\omega_h^2\hat{\mathbf{N}}v^3(t) = \mathbf{0} \ , \\
&\dot{\mathbf{x}}_a - \mathbf{A}_2\mathbf{x}_a - \mathbf{A}_3\dot{\mathbf{x}}_s - \mathbf{A}_4\mathbf{x}_s = \mathbf{0} \ , \\
&\mu_n\left(\ddot{v}(t) + \hat{\mathbf{N}}^T\ddot{\mathbf{x}}_s\right) + 2\theta_n\zeta_h\omega_h\dot{v}(t) + \gamma_n\omega_h^2 v^3(t) = 0 \ ,
\end{aligned} \tag{2}$$

where $\mathbf{x}_s = [\xi(t) \quad \alpha(t)]^T$ is the airfoil displacement vector, $\mathbf{x}_a = [\bar{x}(t) \quad \dot{\bar{x}}(t)]^T$ refers to the augmented aerodynamic states vector, $\hat{\mathbf{N}} = [1 \quad -\delta_n]^T$, $\mathbf{M}_T = \mathbf{M}_s - \mathbf{M}_{nc}$, $\mathbf{B}_T = \mathbf{B}_s - \mathbf{B}_{nc} - \mathbf{B}_c$, and $\mathbf{K}_T = \mathbf{K}_s - \mathbf{K}_{nc} - \mathbf{K}_c$ are the respective mass, damping, and stiffness matrices with the respective contributions from the structure (the s subscript denotes a structural term) and from the unsteady aerodynamic terms (where nc refers to a non-circulatory aerodynamic terms and c the circulatory ones); $\mathbf{A}_i$ (for $i = 1, \ldots, 4$) denotes the aerodynamic coefficient matrices. The full set of matrices is detailed in Appendix A.

When analyzing a typical section with no NES, the terms with a subscript n become null (damping and stiffness), except for the NES mass. Therefore, the set of Eqs. (1) is modified with the removal of the last two terms to the left of the equal sign on the first two equations, as well as the last equation completely.

3. RESULTS

The following analysis was performed by numerically simulating the set of Eqs. (2). A comparison between how the model performs with and without a coupled NES is presented first. A second study concerns a verification of the NES parameters and their influence on the flutter onset speed. A reference aeroelastic model is considered, where the parameters are shown in Table 1a. Table 1b presents the values of the NES parameters, which were assessed by a trial and error procedure.

Table 1: Parameters for numerical simulation.

(a) Typical aeroelastic section

Parameters	Values
b	0.5 m
a	-0.15
ρ	1.0 kg/m^3
m	20.0 kg/m
ω_h	2π rad/s
ω_α	6π rad/s
x_α	0.25
r_α	0.75

(b) Nonlinear energy sink

Parameters	Values
μ_n	0.1
λ_n	0.5
γ_n	1000
δ_n	1.2

3.1 Influence of the NES

Using the parameters in Table 1a, the critical flutter speed was determined through the eigenvalues of the system state matrix. The critical flutter speed is $U_f = 26.8913$ m/s, thereby meaning that for airspeed higher than U_f divergent responses occur.

Numerical simulations of the coupled model were performed by integrating the equations of motion in time (time step of 10^{-3} second) with a Runge-Kutta method and adopting zero initial conditions, except for the pitch angle, which is taken as $\alpha(0) = 1^\circ$. Figure 2 presents the airfoil aeroelastic response with and without NES at the flutter onset speed. The plunge and pitch responses clearly show the benefits of the NES to suppress the flutter instability. Moreover, the NES response indicates that this device successfully drained energy of the airfoil, which caused the end of vibrations.

Typical NES influence in dynamic systems is recognized through suppressing vibrations and to provide smooth transient to nonlinear vibrations in the form of limit cycle oscillations. Here, this phenomenon can be observed as the airspeed increases from U_f. Numerical simulations for velocities progressively higher than U_f were performed to determine the maximum speed where the NES is still effective in holding the airfoil to respond in divergent way. Figures 3 to 5 show the plunge and pitch responses for simulations with $U = 27.5$, 29.0, and 30.85 m/s, respectively. For $U > 30.85$ m/s, the airfoil with NES diverges.

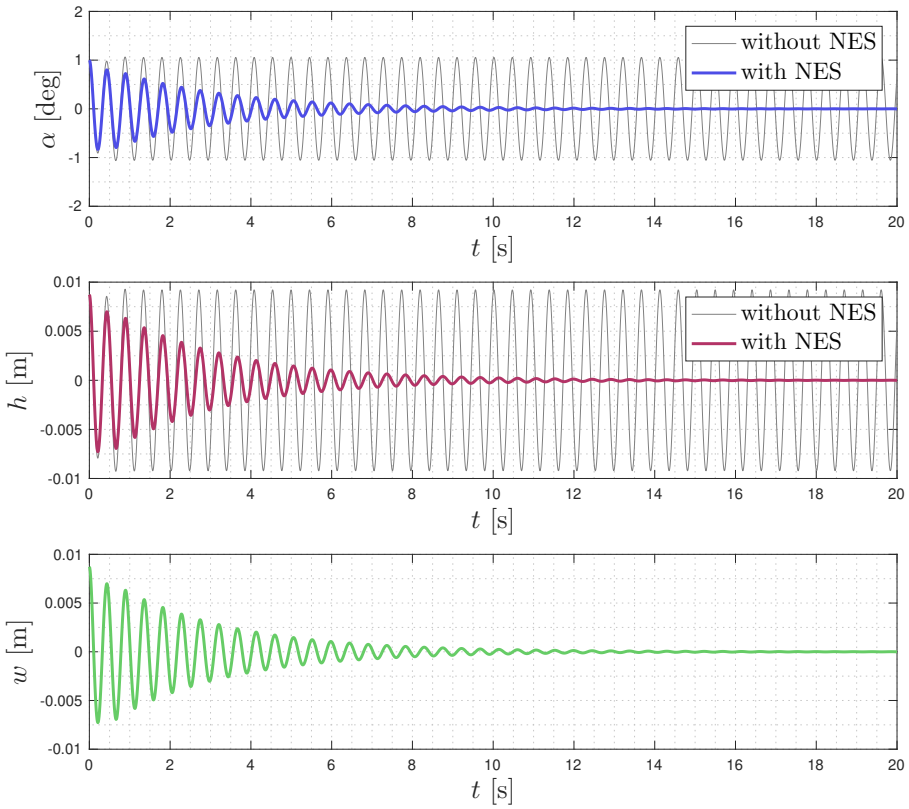

Figure 2: Time responses of the airfoil with and without NES for $U = 26.8913$ m/s (U_f).

Figures 3 to 5 also demonstrate that the NES is responsible to lead the airfoil response to limit cycle oscillations. For $U = 27.5$ m/s $> U_f$, the time responses show that the airfoil flutters with moderate amplitudes, therefore, in a relatively safe condition. Without the NES device, the airfoil in the same conditions would experience divergent motion leading to catastrophic structural failure. The same situation is observed for $U = 29.0$ m/s (*cf.* Fig. 4) and $U = 30.85$ m/s (*cf.* Fig. 5), which demonstrate that the NES can enlarge the speed range for safer airfoil LCO.

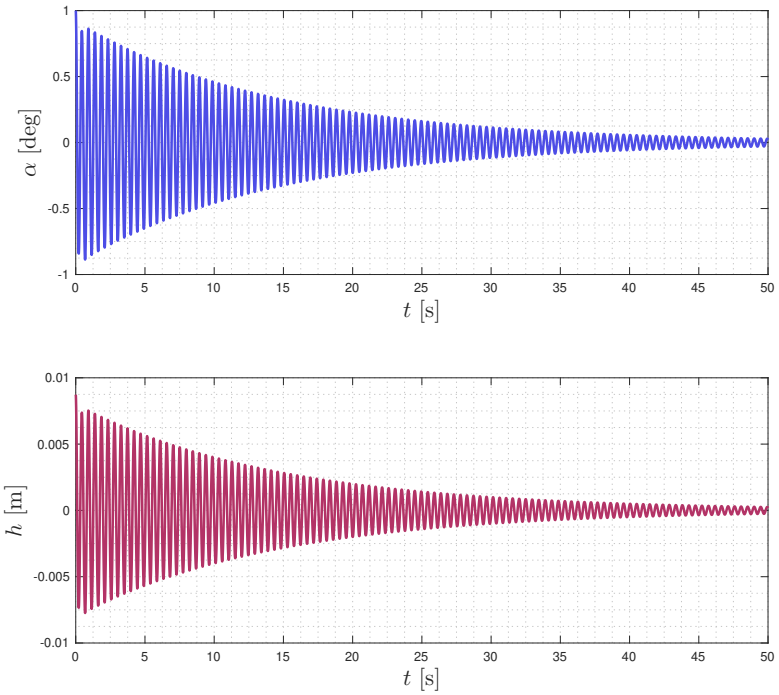

Figure 3: Time responses of the airfoil with NES for $U = 27.5$ m/s.

A range of plunge and pitch frequencies are examined for the cases with and without NES, revealing the results in

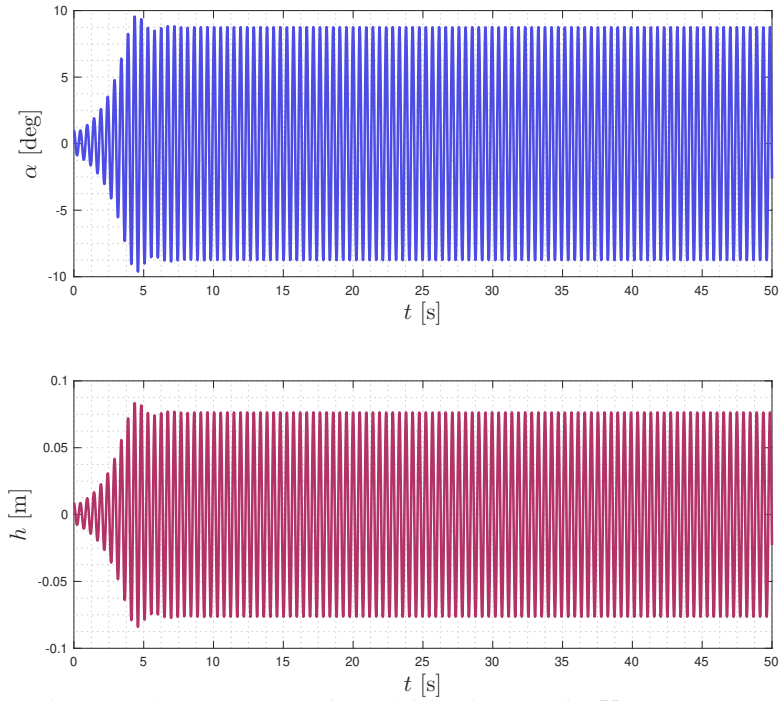

Figure 4: Time responses of the airfoil with NES for $U = 29.0$ m/s.

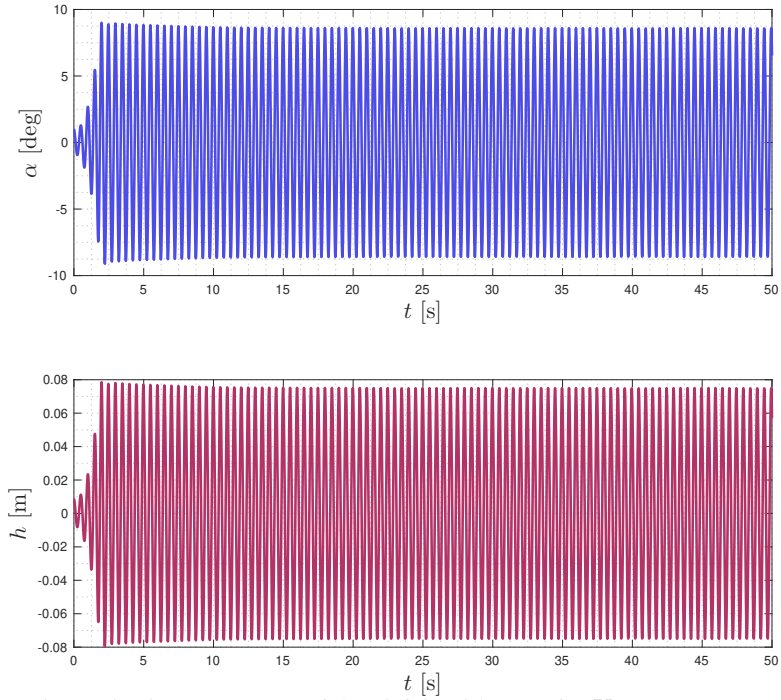

Figure 5: Time responses of the airfoil with NES for $U = 30.85$ m/s.

Fig. 6. Both cases show the trend observed in Fig. 2, confirming that the flutter onset speed is increased due to the NES influence. The use of a NES device is effective for typical aeroelastic sections, but there is room for further improvements. A parametric analysis is a starting point for, potentially, an optimization routine in the future.

3.2 Parametric Study

The parametric study is based on varying the uncoupled plunge and pitch frequencies while keeping the other parameters fixed. Figures 7 and 8 display the flutter speed against a range of ω_h and ω_α variation. According to the order shown in Tab. 1b, two of the parameter variations are presented. The parameters have one value above and one below the reference case in Tab. 1b. The parameters γ_n and μ_n presented no significant variation from its original value, therefore, with inexpressive impact to the flutter onset. For μ_n, it was observed an average of 0.01 m/s of enhancement for a

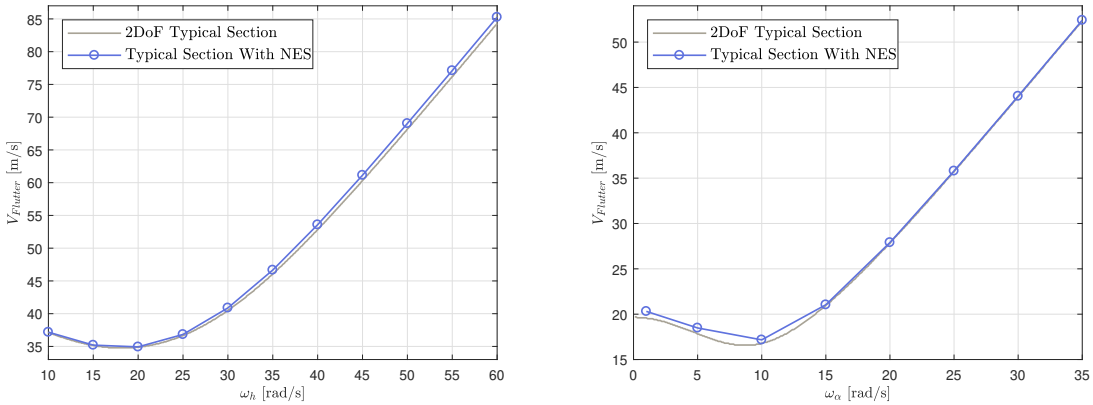

(a) Airfoil plunge response. (b) Airfoil pitch response.

Figure 6: Comparison between the flutter speed of the airfoil with and without a NES varying plunge and pitch frequencies

NES weighing 20% of the airfoil mass, which is already a very significant portion. Increasing μ_n above that could mean notable results yet building a heavier device makes it highly impractical for it to be conceived. Building a relatively stiff NES (higher γ_n) to try and raise the flutter speed is likely to encounter the same issues.

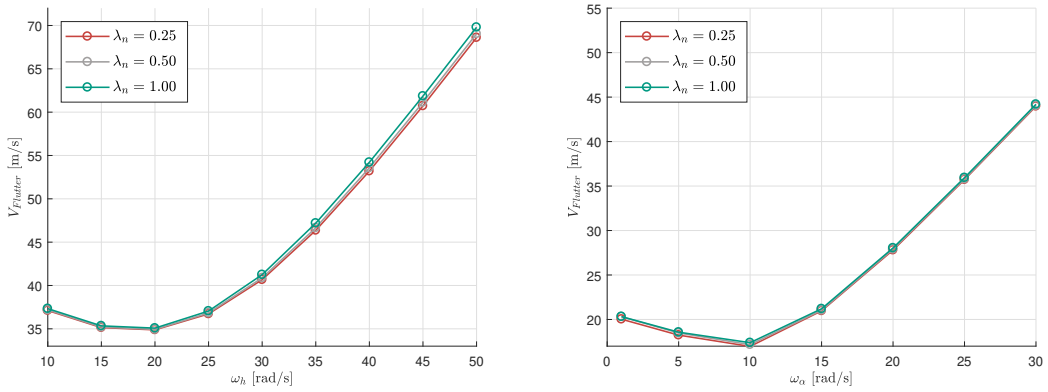

(a) Variating ω_h for $\omega_\alpha = 8\pi$ rad/s (b) Variating ω_α for $\omega_h = 4\pi$ rad/s

Figure 7: Curves for λ_n values

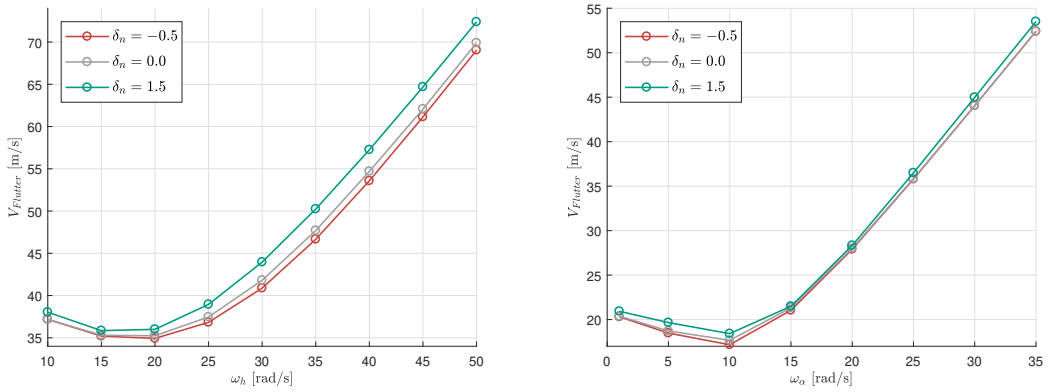

(a) Variating ω_h for $\omega_\alpha = 8\pi$ rad/s (b) Variating ω_α for $\omega_h = 4\pi$ rad/s

Figure 8: Curves for δ_n values

4. CONCLUSIONS

The paper investigated the application of a nonlinear energy sink to the passive control of the flutter onset speed. The typical aeroelastic model was used and coupled with a NES equation for pure cubic stiffness term. Numerical simulation of the resulting set of equations of motion was performed. The present model considers a full linear unsteady aerodynamic loading representation in state space form.

Results comprise a study of the impact of the NES inclusion to the aeroelastic system and the influence on the flutter onset speed and subsequent nonlinear response in post-flutter with NES. It is observed that the NES can increase the critical flutter speed for a reasonable range of aeroelastic parameters. The NES position is the most impacting parameter towards increasing the flutter speed. The typical section with NES has its flutter speed increased, but after a certain value the responses start to present limit cycle oscillations (LCO). The LCO has small amplitudes in both pitch and plunge motions, which indicates that benign nonlinear behavior can also be achieved.

The use of coupled NES to aeroelastic systems seems to be a reasonable form to passively control the flutter onset. Further investigation comprises a complete analysis of typical sections with control surface and NES design for optimal flutter control.

5. ACKNOWLEDGMENTS

The authors acknowledge the financial support for this investigation from the Brazilian's National Council for Scientific and Technological Development (CNPq grants #306824/2019-1 and #134625/2020-0), and the São Paulo State Research Foundation (FAPESP grant #2019/05410–9).

6. REFERENCES

Al-Shudeifat, M.A., 2014. "Highly efficient nonlinear energy sink". *Nonlinear Dynamics*, Vol. 76, No. 4, pp. 1905–1920.

Fung, Y., 1995. *An Introduction to the Theory of Aeroelasticity*. Dover, New York, USA.

Guo, H., Cao, S., Yang, T. and Chen, Y., 2018. "Aeroelastic suppression of an airfoil with control surface using nonlinear energy sink". *Nonlinear Dynamics*, Vol. 94, No. 2, pp. 857–872.

Lee, Y.S., Vakakis, A.F., Bergman, L.A., McFarland, D.M. and Kerschen, G., 2007. "Suppression aeroelastic instability using broadband passive targeted energy transfers, part 1: Theory". *AIAA Journal*, Vol. 45, No. 3, pp. 693–711. doi:10.2514/1.24062.

Luongo, A. and Zulli, D., 2014. "Aeroelastic instability analysis of nes-controlled systems via a mixed multiple scale/harmonic balance method". *Journal of Vibration and Control*, Vol. 20, No. 13, pp. 1985–1998. doi: 10.1177/1077546313480542.

Nayfeh, A.H. and Balachandran, B., 1995. *Applied Nonlinear Dynamics*. Wiley, New York.

Pacheco, D.R., Marques, F.D. and Ferreira, A.J., 2018. "Panel flutter suppression with nonlinear energy sinks: Numerical modeling and analysis". *International Journal of Non-Linear Mechanics*, Vol. 106, pp. 108 – 114. doi: https://doi.org/10.1016/j.ijnonlinmec.2018.08.009.

Saeed, A.S., Al-Shudeifat, M.A. and Vakakis, A.F., 2019. "Rotary-oscillatory nonlinear energy sink of robust performance". *International Journal of Non-Linear Mechanics*, Vol. 117, p. 103249. doi: https://doi.org/10.1016/j.ijnonlinmec.2019.103249.

Theodorsen, T., 1935. "General theory of aerodynamic instability and the mechanism of flutter". Naca report 496.

Tsiatas, G.C. and Charalampakis, A.E., 2018. "A new hysteretic nonlinear energy sink (hnes)". *Communications in Nonlinear Science and Numerical Simulation*, Vol. 60, pp. 1 – 11. doi:https://doi.org/10.1016/j.cnsns.2017.12.014.

Vasconcellos, R., Abdelkefi, A., Marques, F. and Hajj, M., 2012. "Representation and analysis of control surface freeplay nonlinearity". *Journal of Fluids and Structures*, Vol. 31, pp. 79 – 91. doi: https://doi.org/10.1016/j.jfluidstructs.2012.02.003.

7. RESPONSIBILITY NOTICE

The authors are solely responsible for the printed material included in this paper.

A APPENDIX

The matrices presented on the set of Eqs. (2) are:

$$\mathbf{M}_s = \begin{bmatrix} \mu_e & x_\alpha \\ x_\alpha & r_\alpha^2 \end{bmatrix}, \quad \mathbf{K}_s = \begin{bmatrix} \omega_h^2 & 0 \\ 0 & r_\alpha^2 \omega_\alpha^2 \end{bmatrix}, \quad \mathbf{B}_s = \begin{bmatrix} 2\zeta_h \omega_h & 0 \\ 0 & 2r_\alpha^2 \zeta_\alpha \omega_\alpha \end{bmatrix},$$

$$\mathbf{M}_{nc} = -\frac{\rho b^2}{m} \begin{bmatrix} \pi & -\pi a \\ -\pi a & \pi\left(\frac{1}{8} + a^2\right) \end{bmatrix}, \quad \mathbf{B}_{nc} = -\frac{\rho U b}{m} \begin{bmatrix} 0 & \pi \\ 0 & \pi\left(\frac{1}{2} - a\right) \end{bmatrix}, \quad \mathbf{K}_{nc} = \mathbf{0},$$

$$\mathbf{B}_c = (c_0 - c_1 - c_3)\frac{\rho U b}{m}\begin{bmatrix} -2\pi & -2\pi\left(\frac{1}{2} - a\right) \\ 2\pi\left(a + \frac{1}{2}\right) & 2\pi\left(\frac{1}{2} - a\right)\left(a + \frac{1}{2}\right) \end{bmatrix},$$

$$\mathbf{K}_c = (c_0 - c_1 - c_3)\frac{\rho U^2}{m}\begin{bmatrix} 0 & -2\pi \\ 0 & 2\pi\left(a + \frac{1}{2}\right) \end{bmatrix},$$

$$\mathbf{A}_1 = \frac{\rho U^2}{m}\begin{bmatrix} -(2\pi/b)\left[U c_2 c_4 (c_1 + c_3)\right] & -2\pi\left(c_1 c_2 + c_3 c_4\right) \\ (2\pi/b)\left(a + \frac{1}{2}\right)\left[U c_2 c_4 (c_1 + c_3)\right] & 2\pi\left(a + \frac{1}{2}\right)\left(c_1 c_2 + c_3 c_4\right) \end{bmatrix},$$

$$\mathbf{A}_2 = \frac{U}{b}\begin{bmatrix} 0 & 1 \\ -U c_2 c_4 & -(c_2 + c_4) \end{bmatrix}, \quad \mathbf{A}_3 = \begin{bmatrix} 0 & 0 \\ \left(\frac{1}{2} - a\right) & 1 \end{bmatrix}, \quad \mathbf{A}_4 = \frac{U}{b}\begin{bmatrix} 0 & 0 \\ 1 & 0 \end{bmatrix}$$

where $c_0 = 0$, $c_1 = 0.615$, $c_2 = 0.0455$, $c_3 = 0.335$ and $c_4 = 0.3$ are the Wagner function's coefficients based on Sears' approximations (Vasconcellos *et al.*, 2012).